Sensing the Spin of an Individual Ce Adatom

Markus Ternes,[1,2,*] Christopher P. Lutz,[3] Andreas J. Heinrich,[4,5] and Wolf-Dieter Schneider[6,7]
[1]RWTH Aachen University, Institute of Physics, D-52074 Aachen, Germany
[2]Peter-Grünberg-Institute, Forschungszentrum Jülich, D-52425 Jülich, Germany
[3]IBM Almaden Research Center, San Jose, California 95120, USA
[4]Center for Quantum Nanoscience, Institute for Basic Science (IBS), Seoul 03760, Republic of Korea
[5]Physics Department, Ewha Womans University, Seoul 03760, Republic of Korea
[6]Ecole Polytechnique Fédérale de Lausanne (EPFL), Institut de Physique, CH-1015 Lausanne, Switzerland
[7]Fritz-Haber-Institute of the Max-Planck-Society, Faradayweg 4-6, D-14195 Berlin, Germany

(Received 20 August 2019; accepted 1 April 2020; published 22 April 2020)

The magnetic moment of rare earth elements originates from electrons in the partially filled $4f$ orbitals. Accessing this moment electrically by scanning tunneling spectroscopy is hampered by shielding of outerlying orbitals. Here, we show that we can detect the magnetic moment of an individual Ce atom adsorbed on a Cu_2N ultrathin film on Cu(100) by using a sensor tip that has its apex functionalized with a Kondo screened spin system. We calibrate the sensor tip by deliberately coupling it to a well characterized Fe atom. Subsequently, we use the splitting of the tip's Kondo resonance when approaching a spectroscopically dark Ce atom to sense its magnetic moment.

DOI: 10.1103/PhysRevLett.124.167202

Recently, the magnetism of surface-supported rare earth elements has come newly into focus, because individual atoms with $4f$ electrons on ultrathin insulators have been found to show long relaxation times [1], making them interesting candidates for atomic scale memory and possible qubit realization. Because of their large orbital angular momentum, which results in less extended orbitals than the $3d$ orbitals of transition metals like Fe or Co, f orbitals do not usually take part in chemical bonds and only hybridize weakly. This isolation is both a blessing and a curse as this promotes magnetic stability, but at the cost of easy detection and manipulation by electrical means.

Accordingly, scanning tunneling microscopy (STM) and spectroscopy measurements on Ho and Gd adatoms on Pt(111) revealed only low or no detectable interaction cross section between the tunneling electrons and the localized spin [2–4]. Nevertheless, the $4f$ moment of Ho atoms adsorbed on a thin insulating film of MgO on Ag(100) was detected as a change in the electron spin resonance frequency of a single Fe adatom [5] and changed the spectrum of a Co atom in HoCo dimers [6].

Furthermore, in compounds and thin layers of Ce, a lanthanide which hosts only one $4f$ electron, Kondo screening has been observed [7–11]. In Kondo systems, the magnetic moments get compensated by itinerant electrons leading to a highly correlated singlet state and a resonance at the Fermi energy below a characteristic Kondo temperature T_K [12–15]. Kondo features have been found on surface-supported double-decker molecules containing Dy [16], however, measurements on Ce atoms on Ag(111) showed ambiguous results. While first results hinted at Kondo screening [17], subsequent investigations revealed that single Ce adatoms diffuse on the Ag(111) surface even at 4.7 K [18–21] suggesting that the earlier measurement was taken on an immobile Ce cluster and that hydrogenated $4f$ atoms can show low-energy vibrational excitations mimicking a spin signal [22]. However, small Ce clusters showed a clear Kondo resonance [15].

Therefore, we readdressed the question of the magnetic moment of single Ce adatoms by codepositing individual Fe and Ce atoms onto a monolayer of Cu_2N on Cu(100) [23] and performing experiments with a homebuilt STM at $T_{\mathrm{exp}} = 0.7$ K. As shown in Fig. 1(a), single Ce and Fe atoms as well as small clusters formed during deposition at $\approx$10 K are imaged as stable protrusions. The single atoms adsorb on the Cu sites of the Cu_2N [24]. Measuring the differential conductance dI/dV of Fe atoms revealed characteristic features originating from spin-flip excitations [32,33]. To interpret these spectra we use a model Hamiltonian for the magnetic atom,

$$\hat{H}_{\mathrm{imp}} = D\hat{S}_z^2 + E(\hat{S}_x^2 - \hat{S}_y^2) - g\mu_B \vec{B}\,\hat{\mathbf{S}}, \qquad (1)$$

where the spin system is described by the generalized spin operator $\hat{\mathbf{S}} = (\hat{S}_x, \hat{S}_y, \hat{S}_z)$, D and E are the axial and transverse magnetic anisotropy parameters. The Zeeman energy is accounted for with $g \approx 2$ as the gyromagnetic factor, μ_B the Bohr magneton, and $\vec{B}$ the applied magnetic field.

The steplike increase in dI/dV is due to excitations from the ground to energetically higher eigenstates $|\Psi\rangle$ of Eq. (1) via Kondo-like interactions between the localized magnetic

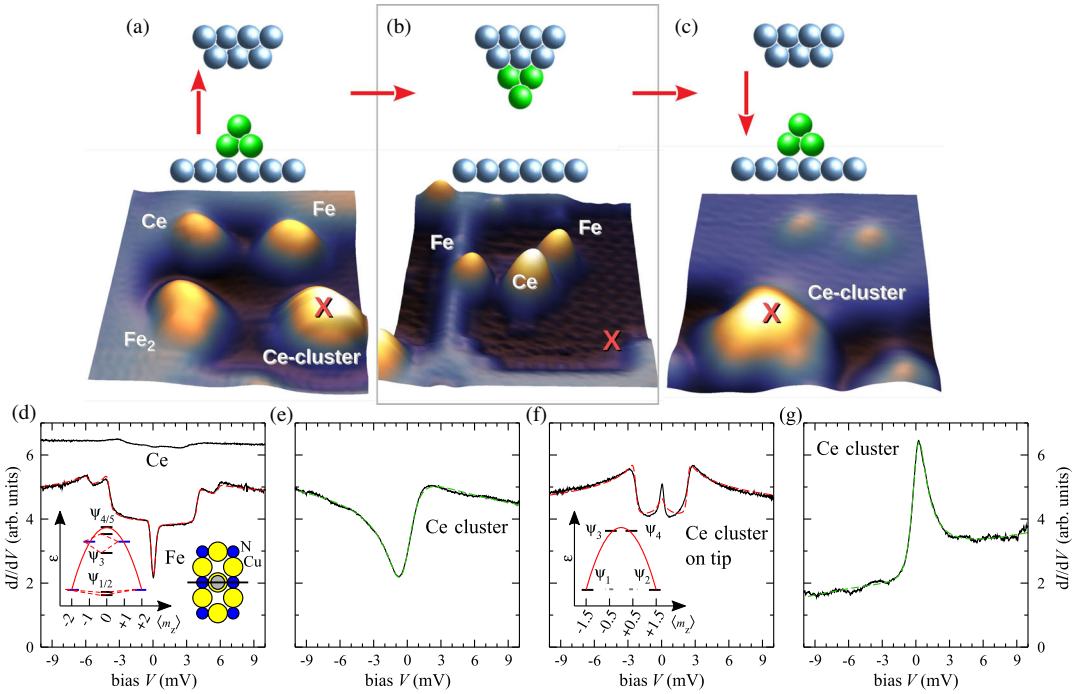

FIG. 1. (a)–(c) Schemes and STM images (5×5 nm^2, $V = 10$ mV, $I = 1$ nA) illustrating the formation of the functionalized tip by picking up ($a \rightarrow b$) and dropping down ($b \rightarrow c$) a small Ce cluster. (d)–(g) Spectra (black lines) and fits using the scattering model (dashed red lines) or a Fano line shape (dashed green lines). (d) Spectrum of a Fe atom with spin $S = 2$ and axial anisotropy along the nitrogen rows of the Cu_2N surface (right inset) with $D = -1.6$ meV, $E = 0.3$ meV (left inset: state diagram), $J\rho_0 = -0.09$ and $U = 0.35$ (bottom), and a Ce atom with flat spectrum (top). (e) Ce cluster showing Kondo resonance having $\Gamma = 1.3 \pm 0.1$ meV, $q \approx 0.45$, and $T_K \approx 15$ K [cross in (a)]. (f) Same Ce cluster after transfer to the tip apex with $S = 3/2$ (inset: state diagram) measured against the bare surface [cross in (b)] and (g) after transfer back to the surface showing again a Kondo resonance having $\Gamma = 0.80 \pm 0.02$ meV, $q \approx 3$, and $T_K \approx 9.3$ K.

moment and the tunneling electron. The tunneling electron has states $|\phi\rangle$ and spin matrices $\hat{\boldsymbol{\sigma}} = (\hat{\sigma}_x, \hat{\sigma}_y, \hat{\sigma}_z)$, leading to the transition matrix elements between initial (i) and final (f) states:

$$M_{i\to f} = \sum_{i',f'} \langle \phi_{f'}, \Psi_f | \left(\frac{1}{2} \hat{\boldsymbol{\sigma}} \cdot \hat{\mathbf{S}} + U \hat{\sigma}_0 \cdot \hat{1} \right) | \phi_{i'}, \Psi_i \rangle. \quad (2)$$

Here, $|\phi_{i'}, \Psi_i\rangle = |\phi_{i'}\rangle |\Psi_i\rangle$ are product states, $\hat{\sigma}_0$ and $\hat{1}$ are identity matrices in their corresponding Hilbert subspaces, and U is a Coulomb scattering parameter which accounts not only for a background dI/dV, but also leads to interference induced bias asymmetries in the spectra, when higher scattering orders are considered [34].

We find an excellent fit to the Fe data using the previously found effective spin $S = 2$, easy-axis anisotropy ($D < 0$) which favors the high magnetic moment along the N rows of the Cu_2N [33], and a transport model which includes scattering processes up to 3rd order in the matrices [34,35] [Fig. 1(d)]. For 3rd order processes, we additionally take the dimensionless coupling $J\rho_0$ into account, where J is the interaction strength between the many electrons of the substrate and the atom's magnetic moment and ρ_0 is the density of states at Fermi energy.

Interestingly, while the dI/dV of Fe atoms show strong steps that indicate spin excitations, single Ce atoms do not. Their spectra are essentially flat and featureless [Fig. 1(d)]. This changes when measurements are taken on a small cluster of Ce atoms [15]. Figure 1(e) shows that we detect an asymmetric feature centered near $V = 0$ which can be well described by a Fano line shape [36,37]:

$$dI/dV \propto \frac{(q + \epsilon')^2}{1 + \epsilon'^2} + (1 + \alpha\epsilon')\rho_0. \quad (3)$$

In this equation, $\epsilon' = (eV - \epsilon_K)/\Gamma$ is the normalized energy where $\epsilon_K \approx 0$ is the position and Γ the half-width of the resonance, q is the Fano parameter, and $(1 + \alpha\epsilon')\rho_0$ accounts for a background dI/dV. We find $\Gamma \approx 1.3$ meV which is due to Kondo screening of the cluster's magnetic moment with $T_K = \Gamma/k_B \approx 15$ K. The $q \approx 0.45$ indicates a relatively strong direct tunneling channel between the tip and the substrate [38]. Because $T \ll T_K$ the cluster is in the strong screening regime [39].

Surprisingly, when we transfer this Ce cluster to the STM tip, by applying $+1$ V bias pulses at close to point contact, the spectrum changes drastically, now revealing a narrow

Kondo resonance, and a spin excitation at about ±2.5 meV [Fig. 1(f)]. This spectrum is typical for an effective $S = 3/2$ system in which the zero-bias Kondo peak originates from scattering between the two degenerate ground states that have weights in the $m_z = \pm 1/2$ projections, and the steps from transitions to states that are energetically higher by $\Delta\epsilon = 2\sqrt{D^2 + 3E^2}$ [inset Fig. 1(f)]. Similar to Fe, this spectrum can be fit with the scattering model even though the central peak is only partly represented, since Kondo screening includes multiple higher-order scattering. This spectrum is very similar to that of a single Co atom on Cu_2N [40–42], but here the magnetic moment originates from the Ce cluster at the apex of the metallic tip, enabling us to exploit it as a mobile sensor as shown below.

Transferring the cluster back to the surface as a control experiment by moving the tip to near point contact and withdrawing while applying $V = -1$ V leads to a similar spectrum as before pickup [Fig. 1(g)]. Both spectra show a Kondo signal, but the transfer of the cluster to a new location on Cu_2N has changed the Kondo signal from dip to a peak. However, Γ is changed only modestly, with T_K changing by about 40%, which might be due to different adsorption geometries [43]. In contrast to the relatively weak coupling of the cluster when attached to the tip apex, the apparently stronger coupling to bulk electrons on the surface quenches the magnetic anisotropy [41,44] and moves the spin system into the strong-coupling Kondo regime.

To characterize the magnetic properties of the Ce cluster at the tip apex, we probe Fe atoms using the Ce-functionalized tip, which results in a complex spectrum [Figs. 2(a) and 2(b)]. Interestingly, the second derivative d^2I/dV^2 closely resembles the convolution of the individual spectra of tip and sample, similar to recent observations of coupled molecular spins in a junction [45]. However, while the convolution yields the correct transition energies, the peak intensities differ significantly between data and convolution [Fig. 2(b)].

This difference has two origins: First, transport which excites both spin systems is complex because the scattering events can occur in different sequences, which must be summed coherently. An electron tunneling from tip (t) to sample (s) can scatter first with the spin on the tip and then with the spin on the surface, and it can also first interact with the surface spin before interacting with the tip spin [Fig. 2(c)]. Destructive quantum interference between these different scattering channels cancels all scattering processes, except those that obey $[\hat{\sigma}_i^t, \hat{\sigma}_j^s]_+ \neq 0$. For spins on tip and surface, this results in a different form for the interaction matrix than Eq. (2), giving [24]:

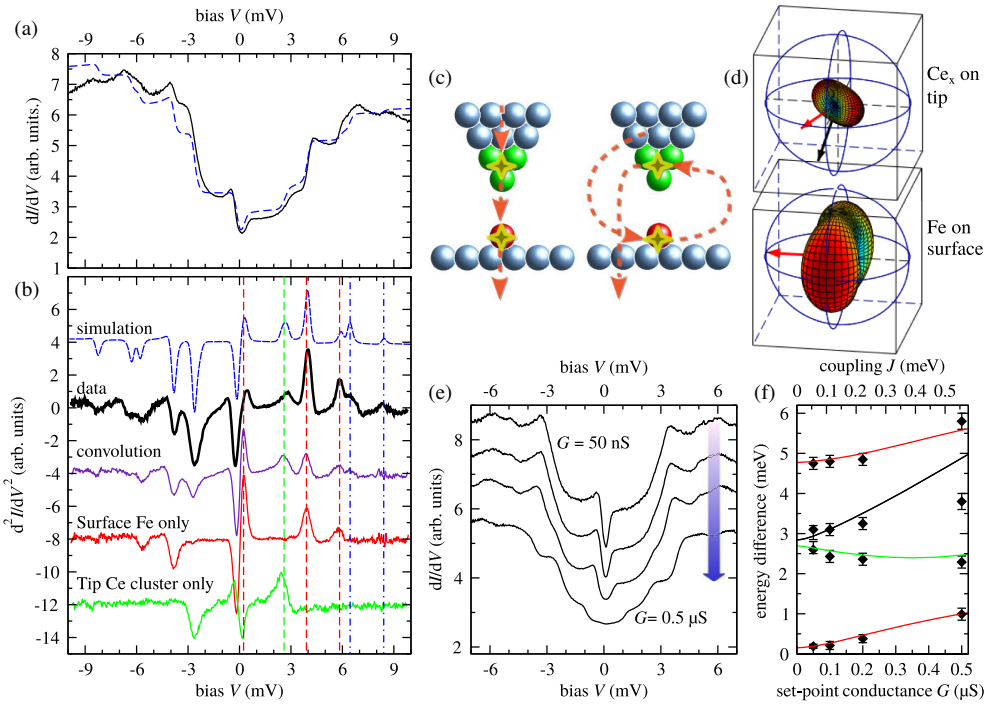

FIG. 2. (a),(b) Spectra measured with the Ce cluster tip against the Fe adatom of Fig. 1(d) (black lines) and simulated curve (dashed blue line). For comparison, spectra of the Ce cluster tip, the Fe adatom, and the convolution of both are shown [vertically shifted colored lines in (b)]. Vertical dashed lines mark transition energies. (c) Scheme of the interaction processes for an electron tunneling from tip to sample. (d) Visualization of the magnetic anisotropy of the Ce cluster and the Fe/Cu_2N surface spin. Red arrows mark the easy axes, while the black arrow marks the intermediate axis of the tip. (e) Set-point dependent spectra (top to bottom: $G = 50$, 100, 200, 500 nS) over a different Fe atom having slightly increased anisotropy parameters ($D = -1.85$ meV, $E = 0.3$ meV). (f) Extracted step positions (symbols) and transition energies of the model calculations using $J^{ts} \propto G$ (lines).

$$M_{i\to f} = \sum_{\substack{j=x,y,z \\ i',f'}} \langle \phi_{f'}, \Psi_f | \Big[U^s \hat{\sigma}_j (\hat{S}^t_j \otimes \hat{1}^s) + U^t \hat{\sigma}_j (\hat{1}^t \otimes \hat{S}^s_j) + \frac{1}{2} \hat{\sigma}_0 (\hat{S}^t_j \otimes \hat{S}^s_j) \Big] | \phi_{i'}, \Psi_i \rangle. \quad (4)$$

Here, the first two terms account for scattering in which spin-spin interaction occurs at only one of the two localized moments, while on the other only a Coulomb-like interaction takes place. The last term accounts for spin-spin scattering on both the tip and sample moments.

Second, while the anisotropy axis of the Fe adatom is well known, the anisotropy axis of the Ce cluster on the tip is unknown and might point in an arbitrary direction. To determine this direction, we use a model that employs Eq. (4) up to 3rd order and a Hamiltonian $\hat{H} = \hat{H}_{\mathrm{Ce}_x} + \hat{H}_{\mathrm{Fe}}$ in which the Ce cluster and the Fe adatom are both described by Eq. (1) using their individually found anisotropy and coupling parameters [24]. This model allows us to determine the relative alignment of the two spins. As illustrated in Fig. 2(d) we find a $\approx 70°$ angle between the two magnetic easy axes. Furthermore, the Ce cluster's magnetic intermediate axis, that is the y direction in Eq. (1), is tilted by only $\approx 18°$ from the surface normal. Note, that the simplicity of the model limits its accuracy [24].

To determine the magnetic coupling between the tip and surface spins, we proceed by changing the set-point conductance $G = I/V$ and consequently the tip-sample distance z. We observe a shift in intensity and energy of the excitations [Fig. 2(e)]. In particular, the energy of the first excitation changes from 0.2 to 1.0 meV, when G is varied by one order of magnitude, i.e., when z is reduced by ≈ 1 Å. This shift can be well described by assuming an antiferromagnetic Heisenberg-like exchange interaction $J^{ts}\hat{\boldsymbol{S}}^t \cdot \hat{\boldsymbol{S}}^s$ between both spins [Fig. 2(f)]. The linear dependence, $J^{ts} = (1.1 \pm 0.2)\ \mathrm{meV}/\mu\mathrm{S} \times G$, implies an exponential dependence on z and points to an orbital overlap as origin of the interaction [46–48].

Having carefully characterized the magnetic tip, we use it to probe spectroscopically "dark" Ce adatoms. Figure 3(a) shows typical spectra, which for small G (tip far from the surface) are almost identical to the ones measured against the bare surface [Figs. 3(a) and 3(b)] except for a slight reduction of the zero-bias Kondo peak height. Prominent differences emerge at increased G. We observe that the central peak becomes asymmetric and for $G \geq 0.15\ \mu$S splits while spectra taken at similar G values on the bare surface do not change significantly [Fig. 3(b)].

This result clearly reveals the presence of a magnetic moment in the Ce adatom that influences the spectrum of the probing tip. We can model the observed behavior by using Eq. (1) and assuming that the spectroscopically dark Ce adatom acts as an effective, set-point dependent, magnetic field oriented in a direction approximately

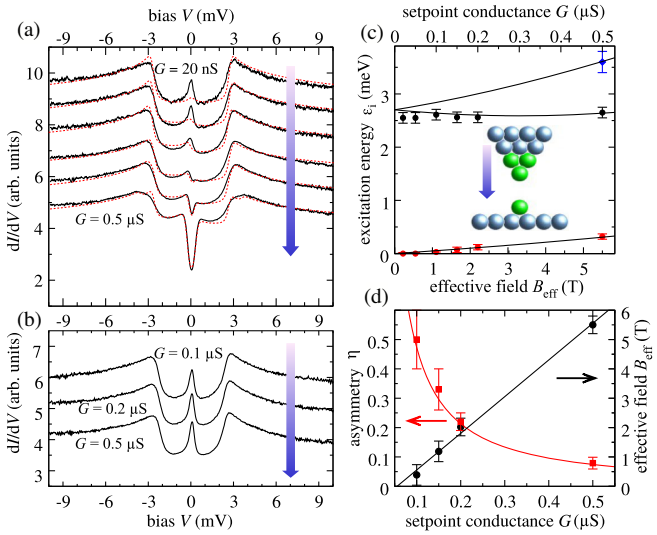

FIG. 3. (a) Spectra (black lines) measured with the functionalized Ce cluster tip positioned above a "dark" Ce adatom with increasing conductance (top to bottom: $G = 20$, 50, 100, 150, 200, 500 nS) and simulations (dashed red lines) using a perturbation model ($S = 3/2$, $D = -1.3$ meV, $E = 0.18$ meV, $J\rho_0 = -0.17$) and a G dependent effective B field. (b) Same tip measured against the bare Cu_2N surface. (c) Extracted step positions (symbols) and calculated transition energies (lines) for different G and B values, respectively. The inset shows schematically the experimental setup. (d) From the data in (a) extracted asymmetry η of the central peak and B field. The lines are guides for the eyes.

out-of-surface having a strength of $B_y \approx (11 \pm 1)\ \mathrm{T}/\mu\mathrm{S} \times G$ [Figs. 3(c) and 3(d)].

While part of the spectral asymmetry can be attributed to Fano-like interference [Eq. (3)], we interpret the asymmetric intensity of the split central feature to originate primarily from an imbalance $\eta = [\rho_0(\uparrow) - \rho_0(\downarrow)]/[\rho_0(\uparrow) + \rho_0(\downarrow)]$ between majority ($\uparrow$) and minority ($\downarrow$) sample states [42,49]. Such polarization can be induced by the spin moment of the Ce adatom [46,47]. The decrease with G suggests an antiferromagnetic interaction as the origin of the exchange field B and the formation of a combined nonmagnetic singlet state of both spins. This indicates a half-integer moment of the Ce adatom and assuming $S = 1/2$, the Ising-like coupling leads to a strength of $J^{ts}_y = (2.5 \pm 0.3)\ \mathrm{meV}/\mu\mathrm{S} \times G$. We found that using isotropic Heisenberg or dipole-dipole interactions instead of Ising interactions leads to much less adequate fits. We also have indications of a reduced tip-adatom interaction strength for Ce adsorbed close to the bare metal [24].

To summarize, our results point to an effective spin $S = 1/2$ of single Ce adatoms on the Cu_2N surface. The very localized $4f$ orbital is inaccessible to ordinary spectroscopy because the interaction cross section with the tunneling electron is too small. This is also the reason for the absence of Kondo screening at our accessible temperatures.

Nevertheless, we sensed the magnetic $4f$ moment by a "detector" spin at the apex of a functionalized STM tip. The particular coupling mechanism between the two spins is not yet fully known, but the observed exponential dependence of the Ising-like interaction points to some $4f$-$5d$ orbital mixing [50].

As a detector we used a Ce cluster which showed a very narrow Kondo resonance at E_F. Such a tip is ideally suited to spin detection, in particular, when T_K is of the order of T_{exp}. Then, the tip shows a clear Kondo resonance at E_F and its sensitivity to exchange interactions and spin polarization is only limited by the unavoidable thermal broadening of the spectra. In contrast, tips with high $T_K > T_{\mathrm{exp}}$ or very low $T_K \ll T_{\mathrm{exp}}$ are contraindicative. While in the former the exchange interaction has first to overcome the Kondo energy $k_B T_K$ before spectral changes can be observed [51], the latter do not show a pronounced resonance. Note, however, magnetic molecules at the tip apex can be exploited in a similar manner as sensor and may be prepared more reproducibly [47,52].

Our results open a new route for studying $4f$ elements on well-defined surfaces. For example, the method outlined here could be used to measure the interactions in artificially created or self-assembled [18,21] atomic or molecular 1D and 2D $4f$ nanostructures.

M. T. acknowledges support by the Heisenberg Program (Grant No. TE 833/2-1) of the German Research Foundation and A. J. H. from the Institute for Basic Science under Grant No. IBS-R027-D1. We thank H.-J. Freund and A. Singha for stimulating discussions.

*Corresponding author.
ternes@physik.rwth-aachen.de

[1] F. Donati, S. Rusponi, S. Stepanow, C. Wäckerlin, A. Singha, L. Persichetti, R. Baltic, K. Diller, F. Patthey, E. Fernandes *et al.*, Science **352**, 318 (2016).
[2] T. Schuh, T. Miyamachi, S. Gerstl, M. Geilhufe, M. Hoffmann, S. Ostanin, W. Hergert, A. Ernst, and W. Wulfhekel, Nano Lett. **12**, 4805 (2012).
[3] T. Balashov, T. Miyamachi, T. Schuh, T. Märkl, C. Bresch, and W. Wulfhekel, Surf. Sci. **630**, 331 (2014).
[4] M. Steinbrecher, A. Sonntag, M. Dos Santos Dias, M. Bouhassoune, S. Lounis, J. Wiebe, R. Wiesendanger, and A. A. Khajetoorians, Nat. Commun. **7**, 10454 (2016).
[5] F. D. Natterer, K. Yang, W. Paul, P. Willke, T. Choi, T. Greber, A. J. Heinrich, and C. P. Lutz, Nature (London) **543**, 226 (2017).
[6] A. Singha, F. Donati, F. D. Natterer, C. Wäckerlin, S. Stavrić, Z. S. Popović, Z. Sljivancanin, F. Patthey, and H. Brune, Phys. Rev. Lett. **121**, 257202 (2018).
[7] F. Patthey, B. Delley, W. D. Schneider, and Y. Baer, Phys. Rev. Lett. **55**, 1518 (1985).
[8] F. Patthey, W. D. Schneider, Y. Baer, and B. Delley, Phys. Rev. Lett. **58**, 2810 (1987).
[9] F. Patthey, J. M. Imer, W. D. Schneider, H. Beck, Y. Baer, and B. Delley, Phys. Rev. B **42**, 8864 (1990).
[10] C. Laubschat, E. Weschke, C. Holtz, M. Domke, O. Strebel, and G. Kaindl, Phys. Rev. Lett. **65**, 1639 (1990).
[11] D. Ehm, S. Hüfner, F. Reinert, J. Kroha, P. Wölfle, O. Stockert, C. Geibel, and H. V. Löhneysen, Phys. Rev. B **76**, 045117 (2007).
[12] J. Kondo, Prog. Theor. Phys. **32**, 37 (1964).
[13] J. Kondo, Phys. Rev. **169**, 437 (1968).
[14] A. C. Hewson, *Kondo Problem to Heavy Fermions* (Cambridge University Press, Cambridge, England, 1997).
[15] M. Ternes, A. J. Heinrich, and W. D. Schneider, J. Phys. Condens. Matter **21**, 053001 (2009).
[16] B. Warner, F. E. Hallak, N. Atodiresei, P. Seibt, H. Prüser, V. Caciuc, M. Waters, A. J. Fisher, S. Blügel, J. Van Slageren *et al.*, Nat. Commun. **7**, 12785 (2016).
[17] J. T. Li, W. D. Schneider, R. Berndt, and B. Delley, Phys. Rev. Lett. **80**, 2893 (1998).
[18] F. Silly, M. Pivetta, M. Ternes, F. Patthey, J. P. Pelz, and W. D. Schneider, Phys. Rev. Lett. **92**, 016101 (2004).
[19] F. Silly, M. Pivetta, M. Ternes, F. Patthey, J. P. Pelz, and W. D. Schneider, New J. Phys. **6**, 16 (2004).
[20] N. N. Negulyaev, V. S. Stepanyuk, L. Niebergall, P. Bruno, M. Pivetta, M. Ternes, F. Patthey, and W. D. Schneider, Phys. Rev. Lett. **102**, 246102 (2009).
[21] M. Ternes, M. Pivetta, F. Patthey, and W. D. Schneider, Prog. Surf. Sci. **85**, 1 (2010).
[22] M. Pivetta, M. Ternes, F. Patthey, and W. D. Schneider, Phys. Rev. Lett. **99**, 126104 (2007).
[23] F. M. Leibsle, S. S. Dhesi, S. D. Barrett, and A. W. Robinson, Surf. Sci. **317**, 309 (1994).
[24] See Supplemental Material at http://link.aps.org/supplemental/10.1103/PhysRevLett.124.167202 for details to the model and additional data, which includes Refs. [25–31].
[25] J. A. Appelbaum, Phys. Rev. Lett. **17**, 91 (1966).
[26] P. W. Anderson, Phys. Rev. Lett. **17**, 95 (1966).
[27] J. A. Appelbaum, Phys. Rev. **154**, 633 (1967).
[28] A. Spinelli, M. Gerrits, R. Toskovic, B. Bryant, M. Ternes, and A. F. Otte, Nat. Commun. **6**, 10046 (2015).
[29] A. A. Khajetoorians, M. Steinbrecher, M. Ternes, M. Bouhassoune, S. Lounis, M. Dos Santos Dias, J. Wiebe, and R. Wiesendanger, Nat. Commun. **7**, 10620 (2016).
[30] D. J. Choi, R. Robles, S. Yan, J. A. J. Burgess, S. Rolf-Pissarczyk, J. P. Gauyacq, N. Lorente, M. Ternes, and S. Loth, Nano Lett. **17**, 6203 (2017).
[31] J. Hermenau, M. Ternes, M. Steinbrecher, R. Wiesendanger, and J. Wiebe, Nano Lett. **18**, 1978 (2018).
[32] A. J. Heinrich, J. A. Gupta, C. P. Lutz, and D. M. Eigler, Science **306**, 466 (2004).
[33] C. F. Hirjibehedin, C. Y. Lin, A. F. Otte, M. Ternes, C. P. Lutz, B. A. Jones, and A. J. Heinrich, Science **317**, 1199 (2007).
[34] M. Ternes, New J. Phys. **17**, 063016 (2015).
[35] M. Ternes, Prog. Surf. Sci. **92**, 83 (2017).
[36] U. Fano, Phys. Rev. **124**, 1866 (1961).
[37] V. Madhavan, W. Chen, T. Jamneala, M. F. Crommie, and N. S. Wingreen, Phys. Rev. B **64**, 165412 (2001).

[38] O. Újsághy, J. Kroha, L. Szunyogh, and A. Zawadowski, Phys. Rev. Lett. **85**, 2557 (2000).
[39] M. Zonda, O. Stetsovych, R. Korytar, M. Ternes, R. Temirov, A. Racanelli, F. S. Tautz, P. Jelinek, T. Novotny, and M. Svec, arXiv:1811.00351v1.
[40] A. F. Otte, M. Ternes, S. Loth, K. Von Bergmann, H. Brune, C. P. Lutz, C. F. Hirjibehedin, and A. J. Heinrich, Nat. Phys. **4**, 847 (2008).
[41] J. C. Oberg, M. R. Calvo, F. Delgado, M. Moro-Lagares, D. Serrate, D. Jacob, J. Fernandez-Rossier, and C. F. Hirjibehedin, Nat. Nanotechnol. **9**, 64 (2014).
[42] K. von Bergmann, M. Ternes, S. Loth, C. P. Lutz, and A. J. Heinrich, Phys. Rev. Lett. **114**, 076601 (2015).
[43] L. Gao, W. Ji, Y. B. Hu, Z. H. Cheng, Z. T. Deng, Q. Liu, N. Jiang, X. Lin, W. Guo, S. X. Du *et al.*, Phys. Rev. Lett. **99**, 106402 (2007).
[44] P. Jacobson, T. Herden, M. Muenks, G. Laskin, O. Brovko, V. Stepanyuk, M. Ternes, and K. Kern, Nat. Commun. **6**, 8536 (2015).
[45] M. Ormaza, N. Bachellier, M. N. Faraggi, B. Verlhac, P. Abufager, P. Ohresser, L. Joly, M. Romeo, F. Scheurer, M. L. Bocquet *et al.*, Nano Lett. **17**, 1877 (2017).
[46] M. Muenks, P. Jacobson, M. Ternes, and K. Kern, Nat. Commun. **8**, 14119 (2017).
[47] B. Verlhac, N. Bachellier, L. Garnier, M. Ormaza, P. Abufager, R. Robles, M. L. Bocquet, M. Ternes, N. Lorente, and L. Limot, Science **366**, 623 (2019).
[48] K. Yang, W. Paul, F. D. Natterer, J. L. Lado, Y. Bae, P. Willke, T. Choi, A. Ferrón, J. Fernandez-Rossier, A. J. Heinrich *et al.*, Phys. Rev. Lett. **122**, 227203 (2019).
[49] S. Loth, C. P. Lutz, and A. J. Heinrich, New J. Phys. **12**, 125021 (2010).
[50] O. Gunnarsson and K. Schönhammer, Phys. Rev. Lett. **50**, 604 (1983).
[51] J. Bork, Y. Zhang, L. Diekhöner, L. Borda, P. Simon, J. Kroha, P. Wahl, and K. Kern, Nat. Phys. **7**, 901 (2011).
[52] G. Czap, P. J. Wagner, F. Xue, L. Gu, J. Li, J. Yao, R. Wu, and W. Ho, Science **364**, 670 (2019).